Available online at www.sciencedirect.com

SciVerse ScienceDirect

Acta Materialia 59 (2011) 7564–7573

Acta MATERIALIA

www.elsevier.com/locate/actamat

Validation of void growth models using X-ray microtomography characterization of damage in dual phase steels

C. Landron [a,b,*], E. Maire [a,b], O. Bouaziz [c,d], J. Adrien [a,b], L. Lecarme [e], A. Bareggi [a,b]

[a] Université de Lyon, CNRS, France
[b] INSA-Lyon, MATEIS UMR5510, 69621 Villeurbanne, France
[c] ArcelorMittal Research, Voie Romaine-BP30320, 57283 Maizieres-les-Metz Cedex, France
[d] Centre des Matériaux, Ecole des Mines de Paris, CNRS UMR7633, BP 87, 91003 Evry Cedex, France
[e] Institute of Mechanics, Materials and Civil Engineering, Université Catholique de Louvain, B-1348 Louvain-la-Neuve, Belgium

Received 3 May 2011; received in revised form 8 August 2011; accepted 28 August 2011
Available online 15 October 2011

Abstract

In situ tensile tests were carried out during X-ray microtomography imaging of three steels: a single phase ferritic steel, a dual phase steel and a fully martensitic steel. Cavity growth was first quantified in the different samples as a function of strain and triaxiality. The Rice and Tracey model, a version of this model corrected by Huang, and a third version accounting for the cavity shape were then used to predict void growth evolution. It was experimentally demonstrated that for steels Huang's correction is a real improvement to the original Rice and Tracey model. Some differences in the void growth kinetic are discussed, accounting for the microstructure and the mechanical behavior of each steel.

Keywords: Steel; Dual phase; Damage; X-ray tomography; Modeling

1. Introduction

A better understanding and modeling of damage phenomena in high strength steels is needed to improve the ductility and properties of these materials. We focus on damage development in a dual phase (DP) steel, one of the most widely used high strength steels. DP steels are composed of a ferritic (soft) matrix containing martensitic (hard) islands. To better understand the fracture of these complex "composite" steels we study the development of damage in the two constituents (ferrite and martensite) separately.

Ductile damage, which leads to the fracture of most metallic materials at room temperature, is a process driven by plastic deformation. It is commonly agreed that this process can be divided into three steps. Void nucleation occurs first and is usually associated with the presence of a second phase, such as particles or inclusions. Cavities frequently nucleate inside the particle or at the particle–matrix interface [1–3]. In a second step the applied plastic deformation induces the growth of the primary nucleated cavities. This phenomenon has, for example, been observed during in situ tensile tests by scanning electron microscopy (SEM) [4]. The third step, coalescence of the nucleated and grown cavities, finally results from the localization of the deformation and the appearance of a crack in the ligament between the cavities. This final step leading to fracture of the material has recently been investigated by Weck et al. [5,6].

Many damage models focus on cavity growth. The first broad family of developed void growth models were simple analytical approaches for isolated voids in a perfectly plastic infinite matrix (see McClintock for cylindrical voids [7] and Rice and Tracey (RT) for spherical voids [8]). This

* Corresponding author at: INSA-Lyon, MATEIS UMR5510, 69621 Villeurbanne, France. Tel.: +33 472437140; fax: +33 472438539.
E-mail address: caroline.landron@insa-lyon.fr (C. Landron).

1359-6454/$36.00 © 2011 Acta Materialia Inc. Published by Elsevier Ltd. All rights reserved.
doi:10.1016/j.actamat.2011.08.046

latter model has been widely used to predict damage growth [6,9–18]. A version of this model accounting for the shape change has also been developed [8,19]. The RT model was later revisited by Huang [20]. These models have been extended by subsequent studies in order to take into account interaction between neighboring voids [21,22] or strain hardening [9,23,24]. A second broad family of more complex void growth models consists of constitutive models for porous elastoplastic or viscoplastic media. The most used of these models is the Gurson approach [25], which has led to various extensions [26–32].

In order to be validated these models outputs must be compared with experimental results. The approach of Worswick et al. [33] is an attempt at this validation. Their approach includes the three damage steps, i.e. void nucleation, void growth and void coalescence, in a general modeling framework and compares each of the three steps with experimental measurements based on the observation of the surface of their samples. Surface observations are experimentally questionable when the quantitative nature of the results is the issue, due, for example, to sample preparation artifacts and, more importantly, to stress relaxation close to the surface (see, for example, Fougères and coworkers [34,35]).

This paper aims at providing some quantitative experimental measurements of the growth step of damage during ductile deformation of steels. For this we used X-ray absorption microtomography, one of the most reliable experimental techniques available, to obtain quantitative three-dimensional (3-D) information on damage [34,36]. Damage in three steels, a fully ferritic, a fully martensitic and a DP steel, was studied by X-ray microtomography during in situ tensile testing of smooth and notched specimens. Quantitative data obtained by this method were then used to validate the different versions of the RT model predicting volume increase and shape change.

2. Experimental methods

2.1. X-ray tomography

X-ray microtomography can now be routinely used for the imaging and quantification of damage in ductile materials [35–37]. The tomography set-up used in the present study was located in the ID15A beam line at the European Synchrotron Radiation Facility (ESRF) in Grenoble, France (more details on the set-up are given in Maire et al. [37]). The tomograph achieves a spatial resolution of 2 μm and a voxel size of 1.6 μm^3 [38]. A dedicated in situ tensile machine described in detail elsewhere was mounted on the rotation stage of the tomograph [39]. Several microtomography scans were performed before and during deformation until fracture of the sample. The strain rate was set to $10^{-3}\ s^{-1}$. During the tomography data acquisition the mobile grip was stopped and maintained at a fixed position. Continuous tensile experiments in tomography are now available [40], but it was demonstrated that the step-by-step procedure used here gives quantitative results similar to those obtained using a continuous loading procedure [41].

2.2. Materials

The three different steels (DP, ferritic and martensitic steels) were cut from 3 mm thick sheets obtained by hot rolling and thermal treatment. Image analysis of optical micrographs of polished surfaces indicated that the DP steel contains about 11% martensite.

Three kinds of specimen shapes, inspired by Bron et al. [42], were cut into each type of steel: a smooth sample; a 2.5 mm radius notched sample (large notch); a 1 mm radius notched sample (small notch). The geometries of the samples are given in Fig. 1. Each initial geometry induced a different initial triaxiality, allowing study of the effects of this key parameter on damage. Only the central area (1.4 mm in height) was imaged during the present study.

2.3. Macroscopic measurements

We have already used X-ray microtomography in order to visualize and quantify damage in DP steel [37,43]. The same procedure was used in the present study. Reconstructed volumes were median filtered. Then they were simply thresholded to differentiate the void phase from the steel phase. On the macroscopic scale the area of minimal cross-section S was first measured to calculate an average value of the true strain in the minimal section of the specimen ε_{loc} at each step using Eq. (1):

$$\varepsilon_{loc} = \ln\left(\frac{S_0}{S}\right) \tag{1}$$

S_0 being the area of the initial cross-section. Note that this expression implies that the effect of porosity on the volume change during straining was excluded.

The minimal cross-section S was also used to evaluate an average value of the true stress in the minimal section:

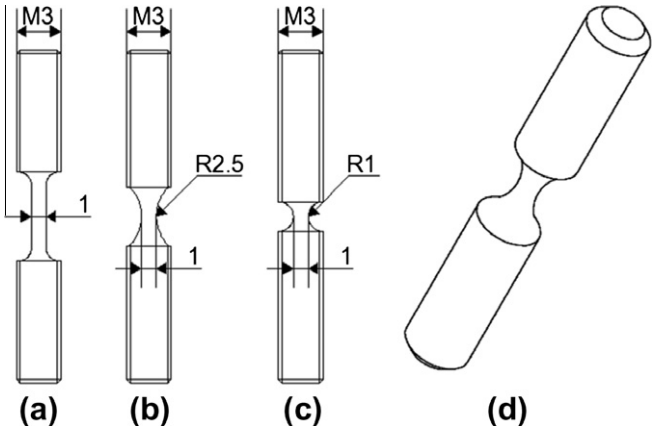

Fig. 1. Tensile samples used: (a) smooth specimen; (b) 2.5 mm radius notched specimen; (c) 1 mm radius notched specimen; (d) 3-D view.

$$\sigma_{true} = \frac{F}{S} \tag{2}$$

F being the measured force during the tensile test.

The curvature radius R_{notch} and the radius of the minimal section a were measured in order to determine the average stress triaxiality T in the center of the minimum cross-section, using the Bridgman formula [44] as reassessed by Wierzbicki and Bao [45].

$$T = \frac{1}{3} + \sqrt{2}\ln\left(1 + \frac{a}{2R_{Notch}}\right) \tag{3}$$

The relevance of these calculated values of ε_{loc} and T was evaluated using finite elements (FE) simulations. The results of the simulations, detailed in Appendix A, show good agreement with the local strain calculated from Eq. (1) and with the stress triaxiality calculated from Eq. (3).

2.4. Microscopic measurements

In a second processing step the central area of the tensile specimen was selected for damage quantification. This sub-region was chosen to be a cubic volume of 300 μm^3, as indicated in Fig. 2a, which shows a transparent view of the external shape of the sample as well as the location of the cavities. It can be assumed that this central sub-region undergoes the highest stress triaxiality state and the highest strain during the tensile test. The size was chosen to be sufficiently large for the elementary volume to be representative but also sufficiently small for the strain and triaxiality to be spatially constant inside this sub-volume. The external shape of three different cavities located inside the sub-region are plotted as a function of deformation in Fig. 2b, showing that in the first steps of deformation cavities remain roughly spherical and only become ellipsoidal later, during the tensile test.

3. Results

3.1. Macroscopic measurements

The force–displacement curves acquired during the in situ tensile test performed on the smooth specimen of each steels are given in Fig. 3a. The slight force relaxation visible on these curves is due to the step-by-step procedure (the displacement was maintained constant and then the force relaxed during the tomographic scan). Fig. 3b shows the tensile true stress of the steels studied as a function of the local tensile true strain. These curves are in agreement with expectations for these materials in terms of strength and ductility. The very high strength and strain shown in

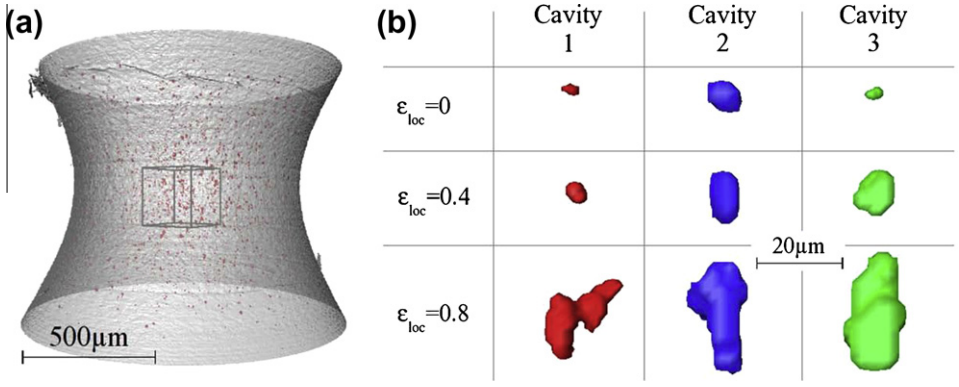

Fig. 2. 3-D views of volumes obtained by tomography: (a) whole sample, with the outer surface shown in light gray and the outer surface of the cavities in dark gray; (b) three chosen cavities selected in the center of the sub-region where the morphology of the cavities was quantified (in the cube shown in (a)) at the center of a DP steel sample at various steps of deformation.

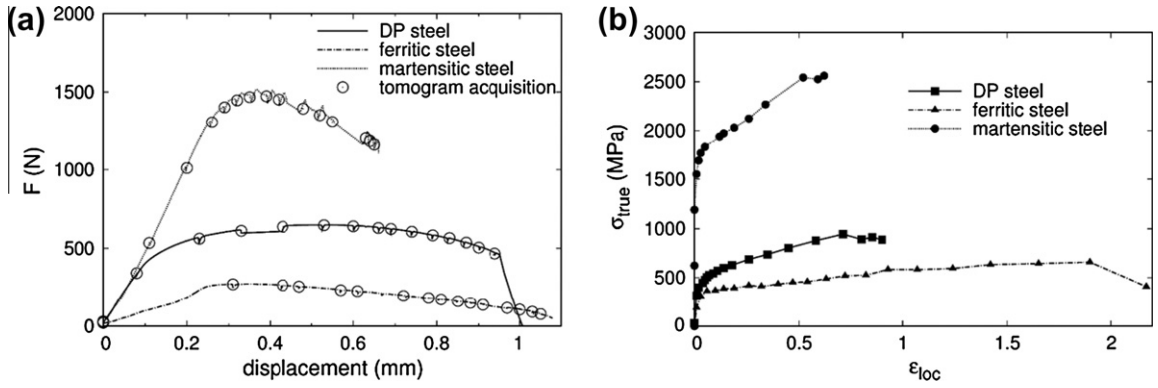

Fig. 3. Mechanical behavior of the three steels in tension: (a) force–displacement; (b) true stress–local true strain.

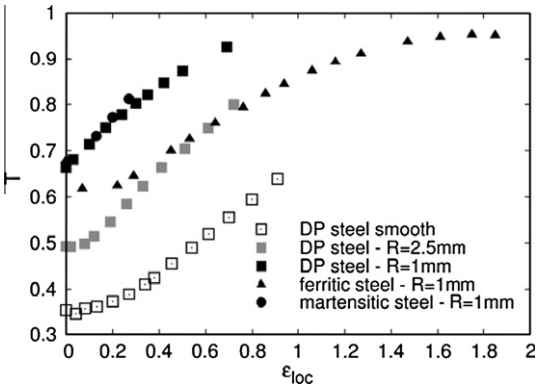

Fig. 4. Triaxiality evolution as a function of the strain in the minimal section during the tensile test in different specimens.

Fig. 3b are due to the processing performed at a very local scale in the present paper. Note also the stress drop at the very end of each curve in Fig. 3b, indicating the onset of macroscopic coalescence.

The evolution of triaxiality during the tensile test of each specimen is calculated from Eq. (3) and is given in Fig. 4. These measured values will later be used in the void growth models. This graph shows two anticipated tendencies: the triaxiality is higher for the smaller notch radius and evolution of the triaxiality is mainly controlled by the plastic strain (evolution is the same for martensite and DP with a 1 mm notch radius). Note that machining of the ferritic 1 mm notch sample was not as perfect as that of the other samples (because ferrite is soft and thus difficult to machine) so this curve deviates slightly from these two general conclusions.

3.2. Microscopic damage measurement

The volume (number of voxels) of each cavity in the subvolume was measured and its equivalent diameter was then calculated assuming a spherical shape. Cavity dimensions in the tensile and transverse directions were also measured to assess the shape change. The absolute error in this measurement is constant (of the order of one voxel). As a consequence, the relative error in measurement of the dimensions depends on the dimensions themselves: it is rather large (100%) when the cavities nucleate (due to the very small size), but then quickly becomes negligible as the cavities grow. Both tomogram processing and cavity analysis were performed with the ImageJ software package [46].

Tracking cavities from one strain step to the next, as in Fig. 2b, proved to be extremely tedious. It can be achieved automatically when the number of objects is constant. This has been used, for instance, in Nielsen et al. [47] and Toda

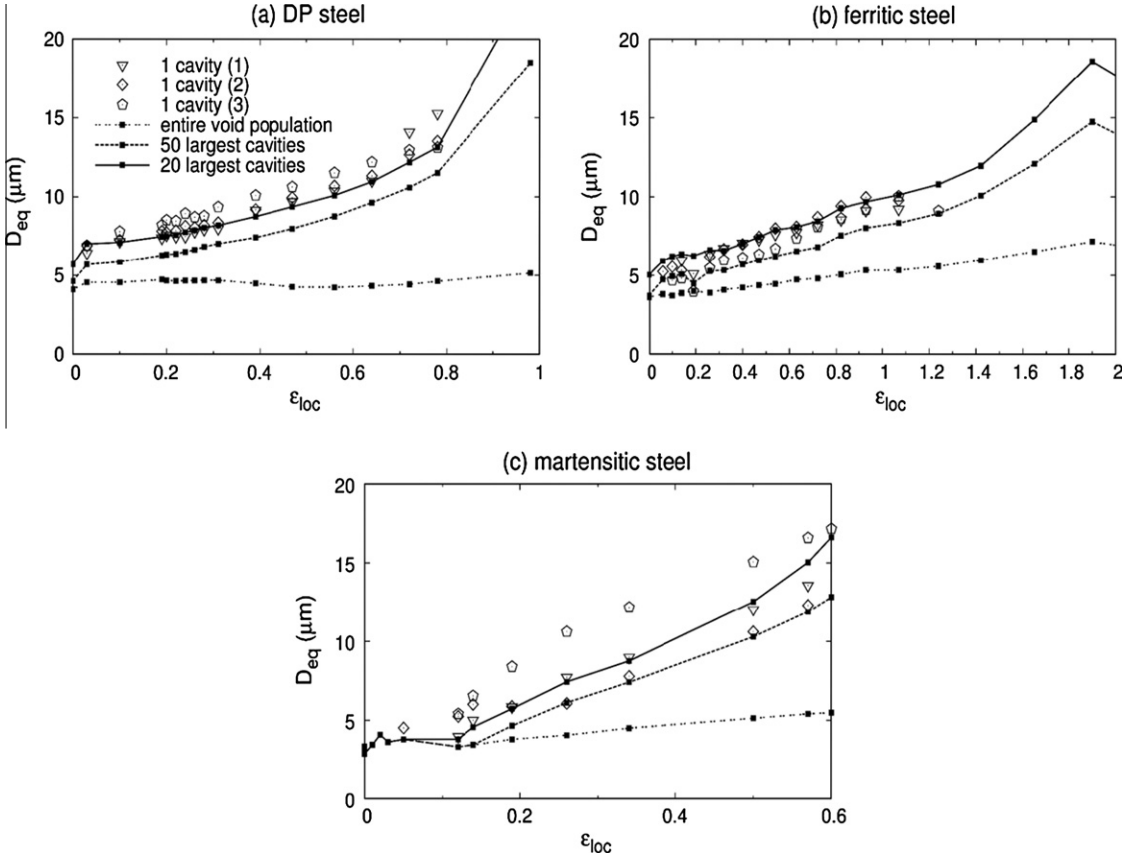

Fig. 5. Evolution of the average void diameter for different numbers of examined cavities: 1, the 20 largest, the 50 largest, and the entire population. The comparison is shown for (a) DP steel, (b) ferrite and (c) martensite.

et al. [48]. In our case, however, the number of objects to be tracked is constantly changing. Tracking was manually performed for a small number of selected cavities for one sample of each material only. These selected cavities were easier to track than others because they were among the largest in the sub-volume.

Another strategy was then adopted to quantify growth more easily and more extensively for all samples. Measurement of the size of the N largest cavities of a population is straightforward [37]. It can be a good measurement of the void growth if these N largest cavities remain the same at each deformation step. This was quantified in the present study for $N = 20$ and $N = 50$ and this was compared with the evolution of the average diameter of the entire population and with the previously mentioned measurement of the three "manually" tracked particles. The results are plotted in Fig. 5. The evolution of diameter closest to the growth measured on single large pores was obtained when using the 20 largest cavities. This experimental strategy has thus been used in the next section.

Regarding these results, two additional remarks can be made.

- The mean equivalent diameter calculated using the entire population remains almost constant in these steels because of the nucleation of new porosities (this has already been measured and explained for DP steels in Maire et al. [37]).
- Void growth acceleration is observed close to the end of the tensile test, due to void coalescence occurring close to the point of fracture of the sample. It corresponds to the value of strain where the stress drop occurs, already mentioned when commenting on Fig. 3b. A local coalescence event between two cavities is qualitatively observable in, for example, Fig. 2b (for cavity 1 at $\varepsilon_{loc} = 0.8$).

In order to characterize evolution of the cavity shape the aspect ratio given by Eq. (4) was calculated for the 20 largest voids for each deformation step.

$$W = \frac{D_{tensile}}{D_{transverse}} \tag{4}$$

where $D_{tensile}$ and $D_{transverse}$ are the void dimensions in the tensile direction and in the transverse direction (average of the two transverse dimensions), respectively. The evolution of W is plotted in Fig. 6 for the three steels studied. Note that whatever the steel, voids are initially isotropic. An optical micrograph taken immediately below the fracture surface of the DP steel specimen is given in Fig. 7. It shows that the main void nucleation mechanism is decohesion of the ferrite–martensite interface. Immediately after nucleation cavities probably have a prolate shape. The size of the voids is very close to the voxel size, so it is experimentally difficult to precisely measure the value of $D_{tensile}$ at the beginning of deformation. As a consequence, cavities artificially appear to be spherical after nucleation. In the case

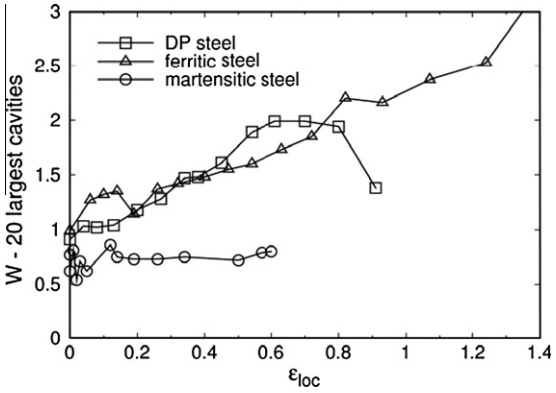

Fig. 6. Evolution of the aspect ratio of the 20 largest cavities in smooth specimens of DP steel, ferrite and martensite.

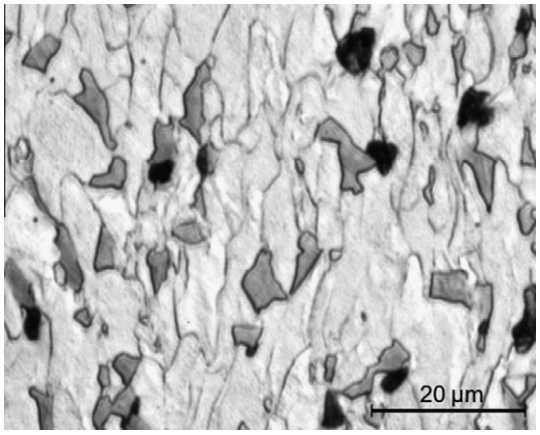

Fig. 7. Optical micrography of a fractured specimen of DP steel. Voids appear in black, ferrite in light gray and martensite in dark gray.

of the DP steel and the ferrite specimens cavities become more and more elongated, while voids in the martensite sample remain slightly prolate during the entire tensile deformation.

4. Modeling and discussion

4.1. Prediction of the equivalent diameter

The RT model [8] is one of the original void growth models. It predicts the growth of an initially spherical cavity in an infinite, rigid, perfectly plastic material subjected to a uniform remote strain field. Assuming a fully isotropic void growth, the variational analysis of Rice and Tracey leads to the following expression for the average rate of growth:

$$\frac{dR}{R} = \alpha_{RT} \exp\left(\frac{3}{2}T\right) d\varepsilon \tag{5}$$

where R is the actual radius of the cavity, ε is the equivalent plastic strain, and α_{RT} is a constant.

A value of $\alpha_{RT} = 0.283$ was first computed by Rice and Tracey [8], later reassessed by Huang using additional

Table 1
Values of the parameters α_{RT} and α_{HUANG} required to fit the models to the experimental data.

	Ferrite		DP steel		Martensite	
	α_{RT}	α_{HUANG}	α_{RT}	α_{HUANG}	α_{RT}	α_{HUANG}
Smooth sample	0.20	0.22	0.45	0.55	1.3	1.6
Notched sample $R = 2.5$ mm			0.50	0.55	1.4	1.6
Notched sample $R = 1$ mm	0.21	0.22	0.52	0.55	1.5	1.6

velocity fields [20]. Huang obtained the same result but with α_{RT} depending on the triaxiality for $T < 1$. The expression for the average rate of growth was found to be:

$$\frac{dR}{R} = \alpha_{HUANG} T^{1/4} \exp\left(\frac{3}{2}T\right) d\varepsilon \tag{6}$$

where $\alpha_{HUANG} = 0.427$.

These models were employed to fit the experimental evolution of the average equivalent diameter using the 20 largest cavities. The values of T and ε used were those experimentally measured in the previous section and reported in Fig. 3. A simple fit using the precalculated values of α led to a discrepancy between the measured and calculated evolution of R in the case of the three materials tested because these initial values were computed for a perfectly plastic matrix. Thus we apply a more pragmatic approach, already used by Pardoen and Delannay [9], Kumar et al. [17] and Taktak et al. [18]. The experimental data for the different materials with different initial triaxiality states were fitted to the two models (initial RT and Huang) by changing the value of α. The results of this fitting procedure are given in Table 1. It is shown that whatever the model used the values of the constant α required to fit the experimental values are not equal to the initial values found by Rice and Tracey or Huang. In the case of the RT model the values differ for each material and for each specimen geometry (except for the ferrite samples). In the case of the Huang version of the model the values differ only for each material but remain the same whatever the sample geometry. It is then demonstrated that the Huang correction improves the RT model by capturing the effect of triaxiality induced by the change in specimen geometry. Huang's predictions are plotted in Fig. 8 in comparison with the equivalent experimental measurements. The agreement is good for each material and initial triaxiality.

4.2. Prediction of the cavity shape change during the growth

As mentioned in Section 3, cavities in DP steel and in ferrite tend to evolve into a more ellipsoidal shape, as opposed to cavities in martensite, which remain roughly spherical during tensile deformation. This modification in void shape can be taken into account in the modeling using the general analysis of RT [8,19]. The rate of change of the void radii is:

$$\frac{dR_k}{R} = \frac{dR}{R} + (1 + E_V) d\varepsilon_k \tag{7}$$

where $1 + E_V$ is a void shape growth parameter and k the considered direction (i.e. in the tensile or the transverse direction).

The right side of Eq. (7) is composed of two terms. The first term dR/R is the void growth rate assuming a spherical cavity. Its initial expression is given in Eq. (5). The void shape change is controlled by the second term in Eq. (7) $(1 + E_V)d\varepsilon_k$. Initially $1 + E_V$ was found to be constant and equal to 5/3. Using void cell calculations, Worswick and Pick [49] showed that this parameter could vary according to the equivalent deformation, the stress triaxiality, the initial volume fraction of porosity and the strain hardening exponent.

In order to use this model the transverse deformations ε_x and ε_y were measured on the tomographic scans. These measurements showed that the transverse strain was half of the longitudinal one, so, using our notation:

$$\varepsilon_x = \varepsilon_y = \varepsilon_{transverse} = -\frac{\varepsilon_{loc}}{2} \tag{8}$$

Using the Huang expression for the void growth rate given in Eqs. (6) and (7) the rate change in the void radii in the tensile and transverse directions can be expressed as:

$$\frac{dR_{tensile}}{R} = \alpha_{HUANG} T^{1/4} \exp\left(\frac{3}{2}T\right) d\varepsilon_{loc} + (1 + E_V) d\varepsilon_{loc} \tag{9}$$

$$\frac{dR_{transverse}}{R} = \alpha_{HUANG} T^{1/4} \exp\left(\frac{3}{2}T\right) d\varepsilon_{loc} - \frac{1}{2}(1 + E_V) d\varepsilon_{loc} \tag{10}$$

Eqs. (9) and (10) were used to predict the void shape change during tensile deformation in the smooth and notched specimens of DP steel and ferrite. The values of α_{HUANG} determined in Section 4.1 were used for each material and the parameter $1 + E_V$, assumed to be constant, was taken as a fitting parameter. The predicted evolutions of the void diameters obtained using this approach are compared with the experimental data in Fig. 9 and the values of the parameter $1 + E_V$ used for the fit are found to be equal to 1 in the DP steel specimens and equal to 0.8 in the ferritic steel, i.e. significantly smaller than the 1.6667 predicted by the theory. Note that $1 + E_V = 0$ for the martensitic sample where the cavities remain isotropic.

4.3. Discussion

The differences between the α_{HUANG} values found for the steels studied and that initially proposed by Huang are

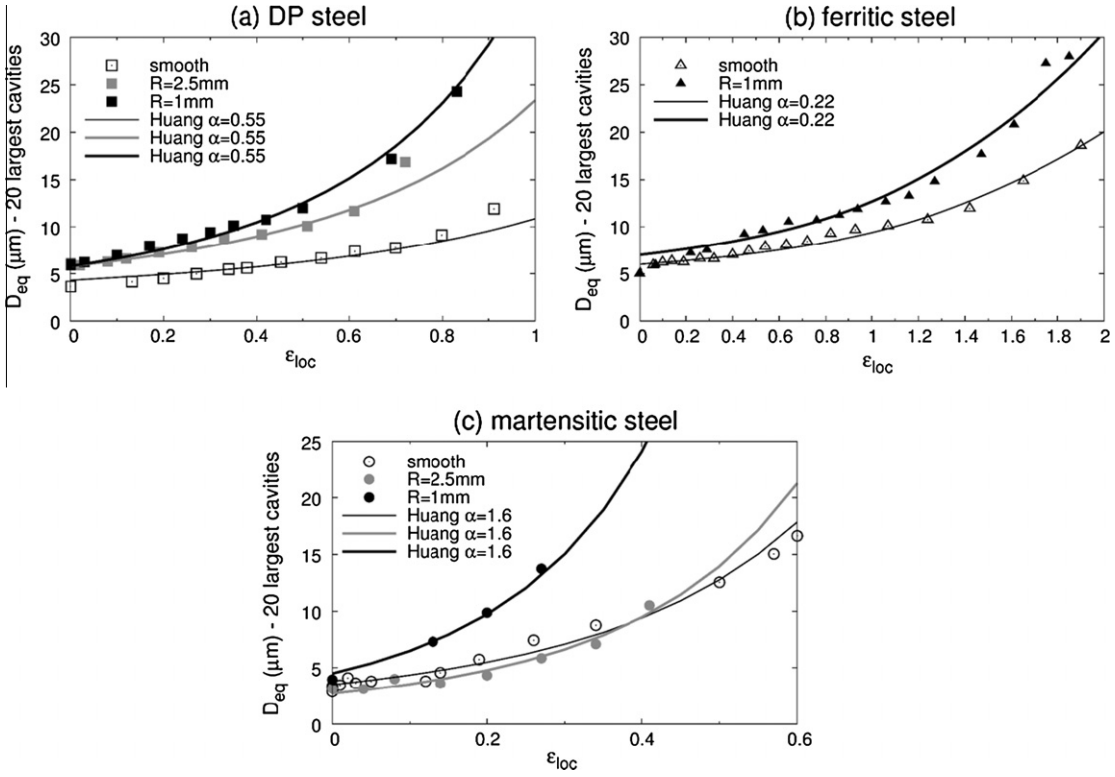

Fig. 8. Comparison of the prediction of the Huang model and evolution of the mean diameter of the 20 biggest cavities measured in (a) DP steel, (b) ferrite and (c) martensite.

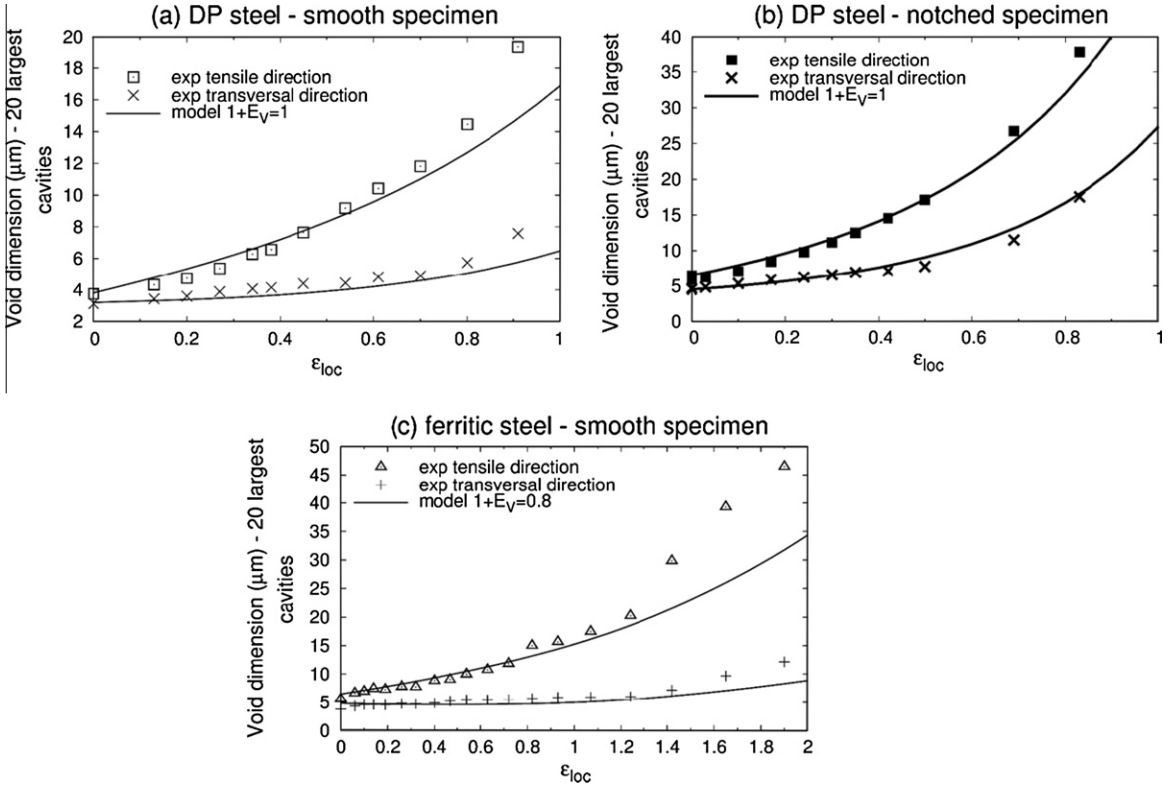

Fig. 9. Comparison of the prediction of the Huang model accounting for shape change and evolution of the dimensions in the tensile and transverse directions of the 20 biggest cavities measured (a) in a smooth DP steel specimen, (b) in a $R = 1$ mm notched DP specimen and (c) in a smooth ferrite specimen.

easily justifiable. The underlying assumptions of Huang's correction are the same as those for the RT model [8,20]. These models predict the isotropic growth of an initially spherical void in an infinite and perfectly plastic matrix. These assumptions were not fully respected in the materials investigated. The differences in the void growth kinetics of the three steels studied, characterized by the different values found for α_{HUANG}, can be explained by the different natures of each material.

In the ferritic steel the α_{HUANG} value was found to be lower than the theoretical one. The most probable cause is strain hardening, which is not included in the model. The effect of isotropic strain hardening on void growth has already been studied [9,23,24], where it was shown that hardening reduces the void expansion rate.

In the DP steel the α_{HUANG} value is higher than in the fully ferritic steel, indicating faster growth with strain. The main difference between the two steels is the presence of a second hard phase inside the DP steel: cavities nucleate close to the martensite islands. These islands prevent the pores from growing in the transverse direction, which is not the case in the ferritic steel samples. Cavities then tend to grow faster in this constrained environment, as shown numerically [50]. Furthermore, with the void density being higher in DP steels, cavities are closer to one another. Consequently, each cavity undergoes more interactions with its neighbors. Void interaction is another reason for faster growth [21,22].

The significant increase in the α_{HUANG} value in the martensite is more difficult to explain. Two assumptions can be made. The first concerns the shape of the voids. In this kind of steel nucleated cavities tend to be more oblate and take the form of microcracks. An aspect ratio of about 0.6 was incidentally measured in Fig. 6. It has been demonstrated that for geometrical reasons such a shape leads to faster void growth [51]. The second possible explanation is related to the nature of strain hardening of the material itself. In martensite a large part of strain hardening is kinematic hardening [52]. It has already been observed in the ferritic steel that isotropic strain hardening leads to a reduction in void growth. Several studies of the kinematic strain hardening effect [28,53] have shown the opposite effect compared with isotropic hardening, i.e. kinematic strain hardening induces void growth acceleration. Note that kinematic hardening should have a less significant effect than isotropic hardening, i.e. cavity growth should remain faster in a perfectly plastic matrix than in a matrix with kinematic strain hardening.

Concerning the change in void shape in the ferritic and DP steels, the values of the parameter $1 + E_V$ found for each material were close to the same. That can be explained by the fact that in the DP steel void growth occurs mainly in the soft phase, i.e. the ferrite, as numerically calculated [54]. The slight difference might be due to the presence of martensite islands. As mentioned earlier, the martensite islands prevent the cavities from growing in the transverse direction, leading to more prolate voids and inducing a higher value of $1 + E_V$ in the case of the DP steel. The values of $1 + E_V$ are found to be lower than that initially determined, indicating that cavities tend to be less prolate in these steels than in a non-hardening matrix. These experimental observations are in disagreement with numerical results from Worswick [49], Ragab [55] and Pardoen [56], which indicated that higher isotopic hardening leads to more prolate cavities.

5. Conclusions

Using in situ tensile tests during X-ray tomography it was possible to obtain quantitative information about damage, in particular about void growth. Concerning this damage stage, we have shown by comparison with careful "manual" single void measurements that study of the mean diameter of the 20 largest pores in the population gives an accurate measurement of the growth of single voids. We have also observed that the void shape changes during the tensile test: cavities, initially spherical, become prolate in the case of ferritic and DP steels.

This experimental data was then used to validate the Huang correction of the RT model on voids having an initial size of a few microns and growing to a size of 30 μm. Thanks to the different triaxiality states, we have shown that accounting for the triaxiality in the initially constant α_{RT} parameter is a real improvement in this void growth model. The general analysis of the RT model accounting for the change in void shape has also been validated. However, some differences in the growth kinetics have been observed for the different steels. These differences are closely linked to the steel microstructure and mechanical behaviors (flow stress and strain hardening mechanisms), which are not explicitly taken into account in these simple analytical models.

Acknowledgements

The authors would like to thank the ESRF for the provision of synchrotron radiation at the ID15A beamline through the ma560 long-term project. The authors also acknowledge Marco Di Michiel for his help as local contact during the experiments performed at the ESRF, and Seabron Adamson for reading the manuscript and improving the English.

Appendix A:. Validation of the values of ε_{loc} and T using finite elements simulations

The average values of the local deformation ε_{loc} and of the stress triaxiality T calculated from Eqs. (1) and (3) were used in the RT and Huang models to predict void growth in the studied steels. In order to evaluate the accuracy of using these values for the local deformation and the triaxiality in the center of the specimen FE simulations were

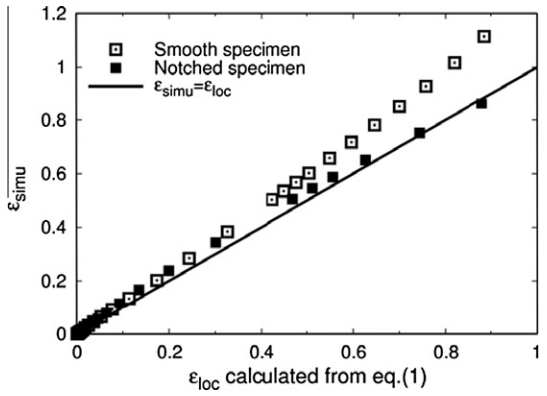

Fig. A1. Comparison of the "experimental" value of ε_{loc} and that calculated using the numerical simulation.

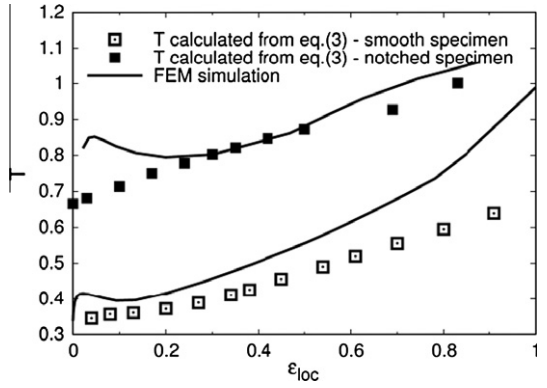

Fig. A2. Comparison of the "experimental" value of the triaxiality and that calculated using the numerical simulation.

performed using the commercial code Abaqus and the open source mesh generator Gmsh [57]. Tensile tests on a smooth specimen and on a notched specimen (with $R_{notch} = 1$ mm) were simulated. The matrix of both specimens is modeled as an isotropic J2 material, with the hardening law given by experimental results for DP steel (see Fig. 3). The local effective strain ε_{simu} and stress triaxiality T_{simu} are extracted from the element located at the center of the minimum section of each specimen. The values obtained from the numerical simulations are compared in Figs. A1 and A2, respectively, with those calculated from the experimental data and using Eqs. (1) and (3). Concerning deformation, the agreement between the analytical solution and the numerical simulation is very good for the notched sample. In the smooth specimen the value calculated for ε_{loc} is lower than that given by the simulation, particularly for values of strain higher than 0.5, but the discrepancy between the two is rather small. Concerning the stress triaxiality, the same conclusion can be drawn: using the value T calculated using Eq (3) and the experimental measurement of the shape of the sample gives an estimation reasonably close to the numerical simulation in our case.

References

[1] Argon AS, Im J. Metall Trans A 1975;6:839–51.
[2] Goods SH, Brown LM. Acta Metall 1979;27:1–15.
[3] Beremin FM. Metall Trans A 1981;12:723–31.
[4] Alexandre F, Deyber S, Vaissaud J, Pineau A. In: Loria EA, editor. Proceedings of the sixth international symposium on superalloys 718, 625, 706 and derivatives, Pittsburgh, PA; 2005. p. 97–110.
[5] Weck A, Wilkinson DS. Acta Mater 2008;56:1774–84.
[6] Weck A, Wilkinson DS, Maire E, Toda H. Acta Mater 2008;56:2919–28.
[7] McClintock FA. J Appl Mech 1968;35:363–71.
[8] Rice JR, Tracey DM. J Mech Phys Sol 1969;17:201–17.
[9] Pardoen T, Delannay F. Metall Mater Trans A 1998;29:1895–909.
[10] Chae D, Koss DA. Mater Sci Eng A 2004;366:299–309.
[11] Rakin M, Cvijovic Z, Grabulov V, Putic S, Sedmak A. Eng Fract Mech 2004;71:813–27.
[12] Hambli R, Mkadem A, Potiron A. J Mater Process Technol 2004;147:302–10.
[13] Dutta BK, Saini S, Navneet A. Int J Pressure Vessels Piping 2005;82:833–9.
[14] Hammi Y, Horstemeyer MF. Int J Plast 2007;23:1641–78.
[15] Wei ZG, Batra RC. Int J Impact Eng 2007;34:1780–96.
[16] Korhonen AS, Manninen T. Mater Sci Eng A 2007;488:157–67.
[17] Kumar J, Srivathsa B, Kumar V. Mater Des 2009;30:1118–23.
[18] Taktak R, Benseddiq N, Imad A. Fatigue Fract Eng Mater Struct 2009;32:525–30.
[19] Thomason PF. Ductile fracture of metals, 1st ed. Oxford: Pergamon Press; 1990.
[20] Huang Y. J Appl Mech 1991;58:1084–6.
[21] Marini B. PhD thesis, Ecole Nationale Superieure des Mines de Paris; 1984.
[22] Marini B, Mudry F, Pineau A. Eng Fract Mech 1985;6:989–96.
[23] Tracey DM. Eng Fract Mech 1971;3:301–15.
[24] Budiansky B, Hutchinson JW, Slutsky DR. Mechanics of solid, the Rodney Hill 60th anniversary volume. Oxford: Pergamon Press; 1982.
[25] Gurson A. J Eng Mater Technol 1977;99:2–15.
[26] Tvergaard V. Int J Fract 1981;17:389–407.
[27] Leblond JB, Perrin G, Devaux J. Euro J Mech Solids A 1995;14:499–527.
[28] Besson J, Guillemer-Neels C. Mech Mater 2003;35:1–18.
[29] Pardoen T, Hutchinson JW. J Mech Phys Solids 2000;48:2467–512.
[30] Benzerga AA, Besson J, Pineau A. Acta Mater 2004;52:4623–38.
[31] Gologanu M, Leblond JB, Devaux J. J Mech Phys Solids 1993;41:1723–54.
[32] Perrin G, Leblond JB. Int J Plast 2000;16:91–120.
[33] Worswick MJ, Chen ZT, Pilkey AK, Lloyd D, Court S. Acta Mater 2001;49:2791–803.
[34] Buffiere JY, Maire E, Cloetens P, Lormand G, Fougères R. Acta Metall 1999;47:1613–25.
[35] Babout L, Maire E, Fougères R. Acta Mater 2004;52:2475–87.
[36] Martin CF, Josserond C, Salvo L, Blandin JJ, Cloetens P, Boller E. Scripta Mater 2000;42:375–81.
[37] Maire E, Bouaziz O, Di Michiel M, Verdu C. Acta Mater 2008;56:4954–64.
[38] Di Michiel M, Merino JM, Fernandez-Carreiras D, Buslaps T, Honkimäki V, Falus P. Rev Sci Instrum 2005;76:043702.
[39] Buffiere JY, Maire E, Adrien J, Masse JP, Boller E. Exp Mech 2010;50:289–305.
[40] Maire E, Carmona V, Courbon J, Ludwig W. Acta Mater 2007;55:6806–15.
[41] Suery M, Adrien J, Landron C, Terzi S, Maire E, Salvo L, Blandin JJ. Int J Mater Res 2010;101:1080–8.
[42] Bron F, Besson J, Pineau A. Mater Sci Eng A 2004;380:356–64.
[43] Landron C, Bouaziz O, Maire E, Adrien J. Scripta Mater 2010;63:973–6.

[44] Bridgman PW. Rev Mod Phys 1945;17:3–14.
[45] Wierzbicki T, Bao Y. Bridgman revisited: on the history effect on ductile fracture. Cambridge, MA: Massachusetts Institute of Technology; 2004.
[46] Abramoff MD, Magelhaes PJ, Ram SJ. Biophotonics Int 2004;11:36–42.
[47] Nielsen SF, Beckmann F, Poulsen HF, Wert JA. Mater Sci Eng A 2004;387:336–8.
[48] Toda H, Maire E, Yamauchi S, Tsuruta H, Hiramatsu T, Kobayashi M. Acta Mater 2011;59:1995–2008.
[49] Worswick MJ, Pick RJ. J Mech Phys Solids 1990;38:601–25.
[50] Staub C, Boyer JC. J Mater Process Technol 1998;77:9–16.
[51] Lassance D, Scheyvaerts F, Pardoen T. Eng Fract Mech 2006;73:1009–34.
[52] Cobo S, Bouaziz O. In: Perez T, editor. Proceedings of the conference on new developments in metallurgy and applications of high strength steels, Buenos Aires; 2008. p. 909–18.
[53] Tanguy B, Besson J. In: Augusti G, Schuëller GI, Ciampoli M, editors. Proceedings of the nineth international conference on structural safety and reliability (ICOSSAR 2005), Rome; 2005. p. 587–90.
[54] Li Z, Guo W. Int J Plast 2002;18:249–79.
[55] Ragab AR. Eng Fract Mech 2004;71:1515–34.
[56] Pardoen T. Comput Struct 2006;84:1641–50.
[57] Geuzaine C, Remacle J-F. Int J Numer Methods Eng 2009;79:1309–31.